Impact of spatial variability in zooplankton grazing rates on carbon export flux

S. A. Meyjes[1], C. M. Petrik[2], T. Rohr[3,4], B. B. Cael[5], A. Mashayek[1]

[1]Department of Earth Sciences, University of Cambridge, Cambridge, UK
[2]Scripps Institution of Oceanography, University of California San Diego, La Jolla, CA, USA
[3]Institute for Marine and Antarctic Science, University of Tasmania, Hobart, Tasmania, 7000, Australia
[4]Australian Antarctic Program Partnership, University of Tasmania, Hobart, Australia
[5]National Oceanography Centre, Southampton, UK

Key Points:

- Inverse modelling predicts strong spatial variability in global grazing dynamics for two zooplankton functional types.
- Locally-tuned zooplankton grazing dynamics improve the model's ability to reproduce satellite-derived phytoplankton biomass.
- Locally-tuned zooplankton grazing dynamics can decrease mean carbon flux by 17% and modify the routing of carbon export.

Corresponding author: Sophie Meyjes, sam296@cam.ac.uk

Abstract

The biological carbon pump is a key controller of how much carbon is stored within the global ocean. This pathway is influenced by food web interactions between zooplankton and their prey. In global biogeochemical models, Holling Type functional responses are frequently used to represent grazing interactions. How these responses are parameterised greatly influences biomass and subsequent carbon export estimates. The half-saturation constant, or k value, is central to the Holling functional response. Empirical studies show k can vary over three orders of magnitude, however, this variation is poorly represented in global models. This study derives zooplankton grazing dynamics from remote sensing products of phytoplankton biomass, resulting in global distribution maps of the grazing parameter k. The impact of these spatially varying k values on model skill and carbon export flux estimates is then considered. This study finds large spatial variation in k values across the global ocean, with distinct distributions for micro- and mesozooplankton. High half-saturation constants, which drive slower grazing, are generally associated with areas of high productivity. Grazing rate parameterisation is found to be critical in reproducing satellite-derived distributions of nanophytoplankton biomass, highlighting the importance of top-down drivers for this size class. Spatially varying grazing dynamics decrease mean total carbon export by >17% compared to globally homogeneous dynamics, with increases in faecal pellet export and decreases in export from algal aggregates. This study highlights the importance of grazing dynamics to both community structure and carbon export, with implications for modelling marine carbon sequestration under future climate scenarios.

1 Introduction

The ocean plays a major role in mitigating the impact of climate change (Hoegh-Guldberg & Bruno, 2010). It is thought that over 20% of anthropogenic carbon dioxide emissions are stored within the global ocean (Friedlingstein et al., 2022). The biological carbon pump describes a suite of processes which can transport organic carbon from the surface ocean, to depths of over 1000m (Turner, 2015). This pathway is responsible for approximately 10% of the ocean's carbon inventory (DeVries, 2022). As carbon dioxide emissions are predicted to increase over the 21st Century, it is essential to fully understand the processes underlying carbon sequestration via the biological pump and predict how they will change in the future (Siegel et al., 2022).

Organic carbon is exported out of the surface ocean as the faecal pellets of consumers or as aggregates of phytoplankton (Siegel et al., 2022). The rate that these forms of particulate carbon are exported via the biological carbon pump is directly influenced by zooplankton grazing. Grazing rates impact the biomass of both predator and prey (Rohr et al., 2023b) and consequently the production of algal aggregates and faecal pellets. Slower grazing rates, for example, reduce the amount of fecal pellets produced by consumers, which decreases the contribution of this pathway to carbon export.

Biogeochemical (BGC) models can estimate particulate carbon using a combination of grazing rates and mortalities (e.g. Aumont et al. (2015)). In BGC models, grazing dynamics between predator and prey can be described by a food limited functional response (Gentleman & Neuheimer, 2008; Anderson et al., 2010; Vallina et al., 2014). This dictates how ingestion rates change with prey density (Gentleman & Neuheimer, 2008). The choice and parameterisation of grazing functional responses can impact estimates of carbon export (Anderson et al., 2010). Holling Type II or Type III (Holling, 1959) grazing formulations are commonly used (Kearney et al., 2021; Rohr et al., 2022). These formulations require two parameters: the maximum grazing rate, g, and the half-saturation constant, k. The half-saturation constant represents the concentration of prey at which half the maximum grazing rate is reached (Gentleman & Neuheimer, 2008). Together these two parameters describe the shape and magnitude of the functional response. Ecologically, they represent the time taken to capture and consume prey (Rohr et al., 2022) – characteristics that vary with

species physiology (Hansen et al., 1997; Hirst & Bunker, 2003). Although the functional response is described by both parameters, population dynamics are most sensitive to change in the k value (Rohr et al., 2022), which is the focus of this study.

Laboratory measurements of k values (Hansen et al., 1997; Hirst & Bunker, 2003) show a large range in k values, spanning 0.96-6000 mgC m^3. Laboratory (Hansen et al., 1997), ecological (Barton et al., 2013) and modelling (Rohr et al., 2023b) studies also point towards strong spatial variability in k values. However, even the most complex BGC models have fixed, globally homogenous, k values. These models can simulate spatial variability in grazing dynamics through the competition of multiple plankton functional types, but this likely does not capture the full physiological variability. Some models use mechanisms such as multi-prey responses (e.g. Anderson et al. (2010, 2015)) and prey preferences (e.g. Aumont et al. (2015)) to further emulate this variability, but these mechanisms are limited and there is little observational data to confirm what emergent grazing dynamics should be (Rohr et al., 2023b). Furthermore, there is uncertainty around the impact of zooplankton grazing on carbon flux, which contributes to the large variability in global estimates of carbon export (Siegel et al., 2014; Boyd, 2015; Rohr et al., 2023b).

We address these gaps by using an inverse modelling approach to estimate spatial variation in zooplankton k values. We find large variations with notable implications for carbon export. We first describe our approach, then our findings and then the implications of these for our overall understanding of zooplankton and carbon export.

2 Methodology

2.1 Overview

This study builds on the work of Siegel et al. (2014) which used satellite-derived estimates of Net Primary Productivity (NPP) and phytoplankton biomass to predict global grazing rates and subsequent estimates of carbon export. The work by Siegel et al. (2014) was extended by Archibald et al. (2019) to include diel vertical migrations (DVM) by zooplankton, allowing organic particulate to be exported via both passive sinking and the vertical movements of organisms. We modified the model by Archibald et al. (2019) to include explicit grazing and zooplankton biomass pools.

Here, we use a 0-D BGC box model to infer the optimal k parameters for both microzooplankton and mesozooplankton, within each grid cell of a 1x1 degree global domain. We force this model with observed bottom-up controls (phytoplankton cell division rates) but allow it to prognostically compute Net Primary Productivity (NPP), phytoplankton biomass, zooplankton biomass and carbon export. Phytoplankton and zooplankton biomass pools are divided into two functional groups each (2P2Z). We then run a suite of simulations to determine what combination of k values is required to best match satellite derived phytoplankton biomass and thus infer the spatial distribution of grazing dynamics. Finally, to understand how more realistic zooplankton behavioural diversity influences marine carbon cycling, we compare global prognostic ecosystem biomass and carbon export from three model scenarios: a run using non-optimised, globally homogenous k values derived from literature (Baseline scenario); a run using optimised, globally homogenous k values (Global-k scenario) and a run using optimised, locally tuned k values (Local-k scenario). The model inputs (§2.2), the ecosystem sub-model (§2.3), the approach to determine optimised k values (§2.4), the carbon export sub-model (§2.5) and results analysis (§2.6) are discussed below.

2.2 Input Data

The model is forced by satellite-derived phytoplankton community mean growth rates, μ. The use of μ ensures coupling between NPP and grazing dynamics. Without this coupling, the top-down influence of grazing dynamics would be removed. This would make

overgrazing of phytoplankton an impossibility, as there would always be NPP regardless of what the free-running biomass population is. μ was selected as an input over the explicit representation of nutrients to ensure observational forcing remained.

In the Carbon-based Productivity Model (CbPMv2) (Westberry et al., 2008), μ is computed from satellite derived chlorophyll-to-carbon ratios (Behrenfeld et al., 2005). Net Primary Productivity (NPP) can then be derived using the relationship between μ and satellite-derived estimates of phytoplankton carbon biomass (P_{obs}), where

$$NPP = \mu P_{obs} \tag{1}$$

In CbPMv2, μ is computed for the bulk phytoplankton population; however, in this study we needed to differentiate the growth rates of two phytoplankton classes, to force our 2P2Z model. The distribution of particle backscatter can partition phytoplankton carbon biomass across size classes, but not their respective growth rates. To estimate the partitioning of growth rates into two size classes (μ_i) we assume a fixed allometric ratio, then determine the values required to produce bulk NPP from the two biomass pools. The following three equations are satisfied at each time step and location:

$$P_{obs} = PS_{obs} + PL_{obs} \tag{2}$$

$$NPP = \mu_{PS}\, PS_{obs} + \mu_{PL}\, PL_{obs} \tag{3}$$

$$\frac{\mu_{PL}}{\mu_{PS}} = \left(\frac{M_{PL}}{M_{PS}}\right)^{-0.25} \tag{4}$$

Both NPP and P_{obs} are derived from monthly climatologies presented in detail in Siegel et al. (2014). These climatologies are then interpolated to produce daily data. NPP values come from the Carbon-based Productivity Model (CbPMv2) (Westberry et al., 2008), which uses observations made by the Sea-viewing Wide-Field-of-view (SeaWiFS) satellite ocean colour mission between 1997 and 2008 (McClain, 2009; Siegel et al., 2014, 2013). Phytoplankton biomass values (P_{obs}) are estimated using particulate backscattering coefficient data (Behrenfeld et al., 2005; Westberry et al., 2008; Kostadinov et al., 2010; Siegel et al., 2013). P_{obs} is partitioned into two size classes (PS & PL) using the slope of the particle size spectrum (Kostadinov et al., 2010; Siegel et al., 2014). M_i represents body size for the two size classes which has an allometric scaling constant of -0.25 applied in accordance with metabolic theory (e.g. West et al. (1997)). This ensures the growth rate of nanophytoplankton is always faster than microphytoplankton. For M_i, the same lower size limit implemented to partition P_{obs} is used, i.e. 20μm and 0.5 μm for PL and PS respectively (Kostadinov et al., 2010; Siegel et al., 2014). A maximum value for μ_i is set at 2 d^{-1} to correspond with the CbPMv2 data (Westberry et al., 2008). Observed minimum growth rates are approximately 0.1 d^{-1}, however the CbPMv2 model extrapolates this towards 0 (Westberry et al., 2008). In our study we use a minimum growth rate within the range of these two values (0.01 d^{-1}).

In the CbPMv2, all properties are assumed to be constant and distributed evenly within the mixed layer (Westberry et al., 2008). Within this study, phytoplankton biomass is assumed to be homogeneous across the mixed layer and negligible below the mixed layer depth as in Siegel et al. (2014). Integrated NPP is assumed constant across the euphotic depth as per Siegel et al. (2014). To enable the calculation of μ, depth integrated NPP is divided by the greater of euphotic zone depth (Z_{eu}) or mixed layer depth (Z_{ml}). Depth data is interpolated from monthly climatologies also presented in detail in Siegel et al. (2014).

2.3 Ecosystem Sub-Model

A simple Phytoplankton-Zooplankton (2P2Z) model is constructed (Table 1). To run the ecosystem model, the global ocean is divided into a 1 degree latitude/longitude grid. The model is only run in grid cells with remote sensing products for a minimum of 10 out of 12 months. This limits the model to roughly between 50 and -50^oN, covering approximately 2.93 $\times 10^8 \text{km}^2$ of the global ocean or just over 80% of its total surface area. This avoids estimation bias in polar regions due to seasonal ice and cloud cover. The model is run with a daily time step and spun up until quasi-equilibrium is reached. Results are taken from the last year of the model run.

The rate of change, per day, in biomass within the mixed layer (Z_{ml}) for each size class is given by

$$\frac{dPS}{dt} = \mu_{PS} PS - G_{ZS} - agg_{PS} PS^2 - m_P(PS - PS_0) - \frac{PS}{Z_{ml}} \frac{dz_{ml}}{dt} H(\frac{dz_{ml}}{dt}) \tag{5}$$

$$\frac{dPL}{dt} = \mu_{PL} PL - G_{ZL,PL} - agg_{PL} PL^2 - m_P(PL - PL_0) - \frac{PL}{Z_{ml}} \frac{dz_{ml}}{dt} H(\frac{dz_{ml}}{dt}) \tag{6}$$

$$\frac{dZS}{dt} = b_{ZS} G_{ZS} - m_{ZS}(ZS - ZS_0) - G_{ZL,ZS} \tag{7}$$

$$\frac{dZL}{dt} = b_{ZL}(G_{ZL,PL} + G_{ZL,ZS}) - m_{ZL}(ZL - ZL_0) - p_{ZL} ZL^2 \tag{8}$$

where PS, PL, ZS, and ZL represent biomass of nanophytoplankton (2-20μm), microphytoplankton (20-200μm), microzooplankton (20-200μm) and mesozooplankton (>200μm) respectively (Moriarty & O'Brien, 2013; Calbet & Calbet, 2008; Sieburth et al., 1978). The model does not resolve vertical or horizontal movement, therefore, biomass represents the mean concentration within the mixed layer, with the assumption of even distribution. Natural mortality (m_i) terms have a lower threshold applied of 0.2 for phytoplankton (Aumont et al., 2015) and 1.0 for zooplankton (Archibald et al., 2019) for model stability. Algal aggregates are represented as quadratic mortality terms (agg_i) of plankton biomass (Aumont et al., 2015). This enables changes in biomass to be reflected in algal export. The influence of shear on aggregate formation (Aumont et al., 2015) is not represented due to the lack of vertical movement and other physical dynamics within the model. The last term in Equations 5 and 6 describes the dilution of biomass as the depth of the mixed layer increases (Archibald et al., 2019; Siegel et al., 2014). H=1 if the change in mixed layer depth is less than or equal to zero, or H=0 otherwise (Archibald et al., 2019; Siegel et al., 2014; Evans & Parslow, 1985). The sub-model is closed by a quadratic mortality term (p_{ZL}) for mesozooplankton, which represents grazing by higher trophic levels.

Zooplankton growth is the product of gross growth efficiency (b_i) and grazing (Anderson et al., 2015). Grazing rates (G_i) are based on Holling Type III (Holling, 1959) functional responses, where

$$G_{ZS} = \frac{g_{ZS}\, PS^2}{k_0^2 + PS^2} ZS \tag{9}$$

$$G_{ZL,PL} = \frac{g_{ZL}\, PL^2}{k_1^2 + PL^2} ZL \tag{10}$$

Table 1. Model variables, parameters and forcing fields.

Parameters

Symbol	Description	Value	Unit	Refs.
dt	Model time step	1	day	-
k_0	Microzooplankton half-saturation constant	-	mgC m^{-3}	-
k_1	Mesozooplankton half-saturation constant	-	mgC m^{-3}	-
b_{ZS}	Microzooplankton gross growth efficiency	0.3	-	(1)
b_{ZL}	Mesozooplankton gross growth efficiency	0.5	-	(2)(3)
g_{ZS}	Maximum grazing rate of microzooplankton	2	d^{-1}	(4)
g_{ZL}	Maximum grazing rate of mesozooplankton	2	d^{-1}	(4)
m_P	Phytoplankton mortality	0.1	d^{-1}	(2)(5)
m_{ZS}	Natural mortality microzooplankton	0.05	d^{-1}	(1)(6)
m_{ZL}	Natural mortality mesozooplankton	0.005	d^{-1}	(1)
PS_0/PL_0	Phytoplankton mortality refuge	0.2	mgC m^{-3}	(1)
ZS_0/ZL_0	Zooplankton mortality refuge	1	mgC m^{-3}	(2)(7)
p_{ZL}	Quadratic mortality mesozooplankton	0.02	$m^3 mgC^{-1} d^{-1}$	(1)(8)
$bact$	Bacterial reminerlisation rate	0.025	d^{-1}	(1)
agg_i	Phytoplankton aggregation term	0.01/0.03	$m^3 mgC^{-1} d^{-1}$	(9)(10)
p_{dvm}	Proportion of mesozooplankton that migrate	0.5	-	(2)
m_{fec}	Fraction of grazing going into fecal flux	0.3	-	(2)(5)
f_{met}	Fraction of absorbed carbon metabolized	0.5	-	(2)(11)

Forcing Fields

Symbol	Description	Unit	Refs.
Z_{ml}	Mixed layer depth	m	(2)(5)
Z_{eu}	Depth of euphotic layer	m	(2)(5)
μ	Phytoplankton Growth Rate	d^{-1}	(12-14)

Prognostic Variables

Symbol	Description	Unit
NPP	Net Primary Productivity	mgC $m^{-2} d^{-1}$
PS	Nanophytoplankton biomass	mgC m^{-3}
PL	Microphytoplankton biomass	mgC m^{-3}
ZS	Microzooplankton biomass	mgC m^{-3}
ZL	Mesozooplankton biomass	mgC m^{-3}
G_{ZS}	Microzooplankton grazing rate on Nanophytoplankton	mgC $m^{-3} d^{-1}$
$G_{ZL,PL}$	Mesozooplankton grazing rate on Microphytoplankton	mgC $m^{-3} d^{-1}$
$G_{ZL,ZS}$	Mesozooplankton grazing rate on Microzooplankton	mgC $m^{-3} d^{-1}$
G_{ZL}	Mesozooplankton combined grazing rate	mgC $m^{-3} d^{-1}$
F_{eu}	Total POC flux out of the euphotic zone	mgC $m^{-2} d^{-1}$
F_{alg}	Flux of algal aggregates out of the euphotic zone	mgC $m^{-2} d^{-1}$
F_{fec}	Flux of fecal pellets out of the euphotic zone	mgC $m^{-2} d^{-1}$
J_{dvm}	DVM-mediated export flux	mgC $m^{-2} d^{-1}$
J_{met}	Respired DIC produced in twilight zone by migrating ZL	mgC $m^{-2} d^{-1}$
J_{fec}	Faecal pellets produced in twilight zone by migrating ZL	mgC $m^{-2} d^{-1}$
ER	Export Ratio	-
DER	DVM Export Ratio	-
DRR	Respiration Ratio	-
RD	Weighted depth of respiration	-
f_{fec}	Fraction of fecal pellets in the euphotic zone	-
p_{met}	Fraction of metabolism in the twilight zone	-

(1) Aumont et al. (2015) (2) Archibald et al. (2019) (3) Anderson et al. (2010) (4) Rohr et al. (2022) (5) Siegel et al. (2014) (6) Walker et al. (2019) (7) Stock and Dunne (2010) (8) Anderson et al. (2015) (9) Stock et al. (2020) (10) (Bisson et al., 2020) (11) Steinberg and Landry (2016) (12) Behrenfeld et al. (2005) (13) Westberry et al. (2008) (14) Kostadinov et al. (2010)

$$G_{ZL,ZS} = \frac{g_{ZL}\, ZS^2}{k_1^2 + ZS^2} ZL \tag{11}$$

k_0 and k_1 are half-saturation constants and g_i are maximum grazing rates. There is no prey preference (Aumont et al., 2015) for mesozooplankton grazing and no multiple prey feeding response (Anderson et al., 2010, 2015) as this fundamentally changes the relationship between k and the prey distribution (Gentleman et al., 2003; Rohr et al., 2022; Anderson et al., 2015). The grazing terms allow for two-way coupling between zooplankton and their prey, so that grazing rates are influenced by both predator and prey biomass. A Type III functional response is chosen due to increased stability, its suitability to coarse resolution global model and improved reproduction of seasonal population dynamics compared to Type II (Rohr et al., 2023b, 2022).

2.4 Optimisation of Grazing Dynamics

This study aims to assess the impact of locally-tuned grazing dynamics on outputs from a coupled ecosystem-carbon export model. To do this three scenarios are considered (§2.1). The same ecosystem-carbon export model and bottom-up forcing is used for all three scenarios and all parameters except k are kept constant. For the Baseline and Global-k scenarios, the same pair of k values is used for every grid cell location (i.e. they are globally homogeneous). For the Baseline scenario, the median k values from 40 models reviewed by Rohr et al. (2022) are used. These are 40 and 80 mgC m^{-3} for microzooplankton and mesozooplankton, respectively. For the Global-k scenario, a single pair of globally optimised values are used. For the Local-k scenario, k values are locally tuned, at every grid cell location. The optimisation process for both the globally optimised pair, and locally-tuned values is detailed below.

For each model grid point, the optimum half saturation constant for both microzooplankton (k_0) and mesozooplankton (k_1) grazing is assessed using an inverse modelling approach. Multiple simulations of the model are run, each with a different set of k_0 and k_1 values. The output of the model is then compared to the climatological seasonal cycle of phytoplankton biomass (Behrenfeld et al., 2005; Westberry et al., 2008; Siegel et al., 2013, 2014). The k values that most closely reproduce these satellite-derived biomass values are then selected as the 'optimum' k values. To find the optimum values, a cost function is used. Several different cost functions were analysed which produced consistent results (Figures S1 & S2). The cost function presented here (Equation 12) is the sum of the normalised absolute average error (nAAE) (Stow et al., 2009) for both nanophytoplankton and microphytoplankton, computed across the full seasonal cycle. This represents the degree of agreement in the size and alignment of the seasonal cycle between model and observations. Here, the term 'observations' refers to the satellite-derived phytoplankton biomass. A value of zero indicates a perfect match and alignment with observations.

$$\text{Cost} = nAAE_{PS} + nAAE_{PL} \tag{12}$$

where,

$$nAAE_{P(i)} = \frac{AAE_{P(i)}}{\sigma_o} \tag{13}$$

$$AAE_{P(i)} = \sum \frac{|P(i)_{obs} - P(i)_{mod}|}{n} \tag{14}$$

σ_o is the standard deviation of the observed data, which represents observed temporal variance in the seasonal cycle; n is the total number of observations across the climatological

year; i is the size class and $P(i)_{obs}$ and $P(i)_{mod}$ are observation and model values of phytoplankton respectively. The absolute average error is normalised by the standard deviation of the observed climatology, to enable comparisons of relative errors in high and low productivity regions. Due to the uncertainty in zooplankton observational estimates (Strömberg et al., 2009) a zooplankton term was not included in the cost function.

To maximise computational efficiency, two routines of k optimisation are carried out. The first coarse resolution routine uses 15 log spaced values of k_0 and k_1 (mgC m^{-3}): 16, 20, 26, 33, 43, 54, 70, 89, 114, 146, 187, 239, 306, 392 and 501. These are within the range of empirical and model estimates presented in Rohr et al. (2022). The model is run for each possible pair of half-saturation constants, at every grid cell (i.e. a total of 225 (15x15) runs at each grid cell). The pair of half-saturation constants that produces the lowest cost are then selected as the optimal values at that location. The result is a distribution of optimal k values across the global ocean.

To improve the resolution of our optimisation, a second optimisation routine is then carried out. At each location, the sampling input of k values is calculated by first taking the optimum k values from the coarse optimisation run. Next, an upper and lower limit for input values is calculated by ± 10 % in each direction from the optimised values. Numbers are rounded to the nearest integer. The model is then run for every pairing of integers between these two limits at that location. The cost function is then reevaluated at each grid cell location and a new optimised pairing of k values selected. For example, if the coarse optimisation identifies $k_0 = 20$ & $k_1 = 26$ as optimal, we then rerun the simulation for all integer values (and pairings) of $18 <= k_0 <= 22$ and $23 <= k_1 <= 29$.

For the Global-k scenario, the globally homogenous pair of k values are estimated by globally integrating the cost function for each k pairing. The pair that produce the lowest cost value from this global integration are selected for the Global-k scenario. The results from the coarse resolution optimisation routine are used for this integration. For the Local-k scenario, the optimum pair of k values estimated for every grid cell (from the second optimisation routine) are used.

2.5 Carbon Export Sub-Model

The Archibald et al. (2019) carbon export model is used to examine the impact of grazing parametrisation in this study. The carbon export model consists of two modules: the euphotic and twilight zone modules. In this study, the twilight zone component has remained unchanged from its description in Archibald et al. (2019). However, a few changes have been made to the euphotic zone module to reflect the use of fully-coupled grazing terms and the use of μ as an input instead of NPP. These changes are described below.

Carbon export out of the euphotic zone (Total Export Flux) is the sum of the passive sinking flux (F_{eu}) and DVM-mediated flux (J_{dvm}).

$$\text{Total Export Flux} = F_{eu} + J_{dvm} \tag{15}$$

$$F_{eu} = F_{alg} + F_{fec} \tag{16}$$

F_{eu} is the sum of microphytoplankton algal aggregates (F_{alg}) and faecal pellets produced by mesozooplankton grazing (F_{fec}). Sinking algal aggregates from the euphotic layer (F_{alg}) are estimated as

$$F_{alg} = Z_{eu}\ (1 - bact)\ (agg_{ZL}\ PL^2 + 0.5\ m_P\ PL) \tag{17}$$

where the microphytoplankton aggregation term and 50 % of microphytoplankton linear mortality contributes to sinking aggregates (Aumont et al., 2015). As in Aumont et al. (2015), the remaining 50 % of the linear mortality term is classed as small POC, which is retained in the euphotic zone. *bact* is the proportion lost to bacterial remineralisation (Aumont et al., 2015). Nanophytoplankton does not contribute to algal export in the model, as its smaller cell size means aggregates are assumed to contribute to the microbial web in the euphotic zone, rather than sinking export flux (Archibald et al., 2019; Calbet & Landry, 2004).

Euphotic zone sinking faecal pellets (F_{fec}) and faecal pellets produced in the twilight (J_{fec}) are estimated as

$$F_{fec} = (p_{dvm}\ f_{fec} + (1 - p_{dvm}))\ (m_{fec}\ G_{ZL})\ Z_{eu} \tag{18}$$

$$J_{fec} = p_{dvm}\ (1 - f_{fec})\ (m_{fec}\ G_{ZL})\ Z_{eu} \tag{19}$$

where G_{ZL} is the combined grazing rate for mesozooplankton on both prey types ($G_{ZL,PL} + G_{ZL,ZS}$), p_{dvm} is the proportion of mesozooplankton that participate in DVM, m_{fec} is the fraction of grazed carbon expelled as faecal pellets and f_{fec} is the proportion of faecal pellets expelled in the euphotic zone. DVM is treated as a single event and particulate organic carbon (POC) is a single pool of carbon that decays exponentially (Archibald et al., 2019). All carbon export parameter values (Table 1) were kept consistent with those detailed in Archibald et al. (2019). In this study, microzooplankton do not vertically migrate and their faecal pellets do not contribute to export flux as their smaller pellet size means they are assumed to be consumed by the microbial loop in the euphotic zone (Archibald et al., 2019; Calbet & Landry, 2004).

Finally, the production of respired dissolved inorganic carbon (DIC) in the twilight zone (J_{met}) is estimated as

$$J_{met} = p_{met}\ p_{dvm}\ f_{met}\ (G_{ZL}\ - m_{fec}\ G_{ZL})\ Z_{eu} \tag{20}$$

where p_{met} is the fraction of total metabolism that occurs in the twilight zone and f_{met} is the fraction of absorbed carbon that is metabolised. The contribution of both J_{met} and J_{fec} to DVM-mediated flux (J_{dvm}) is then described by

$$J_{dvm} = J_{met} + J_{fec} \tag{21}$$

2.6 Analysis

To analyse the output data from the optimisation of grazing dynamics and the ecosystem-carbon export model, several additional metrics are considered.

2.6.1 Grazing Dynamics

The biomass-weighted k value (BW-k) combines both k_0 and k_1 values. It considers the optimal k value for each zooplankton class and their relative abundance at every grid cell location (BW-$k = (k_0\ ZS + k_1\ ZL)/Z$). This reflects the emergent grazing dynamics of the entire zooplankton community. The half-saturation constant and maximum grazing rate can be related to the prey capture efficiency, ε. The prey capture efficiency is calculated by dividing the maximum grazing rate (See Table 2) by the half-saturation constant for each grid cell (Rohr et al., 2022) ($\varepsilon = g\ /\ k^2$). To understand the relationship between k and both NPP and prey biomass, a linear regression is fitted to log-normalised data.

2.6.2 Carbon Export

The export ratio represents the proportion of NPP exported as carbon from the euphotic zone. DVM export ratio (DER) is DVM-mediated export as a fraction of total carbon exported from the euphotic zone. The DVM respiration ratio (DRR) is the amount of respiration carried out by migrating zooplankton as a fraction of the integrated respiration from the twilight zone (Z_{eu} – 1000m). The weighted depth of respiration (RD) is the increase in depth of dissolved inorganic carbon (DIC) production and oxygen utilisation, as a result of zooplankton vertical migrations. Carbon export metrics are described in further detail in Archibald et al. (2019).

3 Results

3.1 Distribution of Locally Tuned Grazing Dynamics

Local tuning of k values results in high variability in inferred grazing dynamics (Figure 1 & S1-4). k values span a range of 537 mgC m^{-3} (Table 2). High k values are generally associated with highly productive regions (Figure 1c). Lower values are generally associated with the less productive subtropical oligotrophic gyres, with the exception of the eastern South Pacific, where maximum k values (551 mgC m^{-3}) are estimated for microzooplankton. Maximum k values are also found in the high latitudes of the southern hemisphere.

Zooplankton functional groups are characterised by different grazing dynamics. Microzooplankton k values estimated from local optimisation are, on average, lower than mesozooplankton (median k values are 18 mgC m^{-3} and 27 mgC m^{-3} respectively), suggesting faster grazing for the smaller size class (Table 2 & S1). In addition, the globally optimised pair of k values (estimated for the Global-k scenario - see §2.4) are 33 mgC m^{-3} and 392 mgC m^{-3} for micro- and mesozooplankton respectively. Microzooplankton are generally characterised by more efficient grazing than mesozooplankton, with the exception of the oligotrophic gyres (Figure S5).

The distribution of grazing dynamics also differs between zooplankton size classes. This is particularly evident in equatorial upwelling regions, where microzooplankton and mesozooplankton communities are characterised by low and high k values respectively (Figure 1a, b). These differences result in divergent relationships between k values, NPP and prey biomass for the two size classes. High k_0 values are associated with low NPP and prey biomass, whilst high k_1 values are associated with high NPP and prey biomass (Figure S6).

Table 2. Locally-tuned microzooplankton (k_0) and mesozooplankton (k_1) half-saturation constants estimated using the cost function. Half-saturation constant values are in mgC m^{-3}. Global-k and Baseline scenario k values are included below for comparison (NB: average statistics cannot be provided for these two scenarios due to the same value being used for every grid cell in the model domain).

Local-k	k_0	k_1
Median	18	27
Geometric Mean	27	38
Biomass-weighted Mean	31	49
Range	14-551	14-551
IQR	17(14-31)	38(14-52)
Global-k	33	392
Baseline	40	80

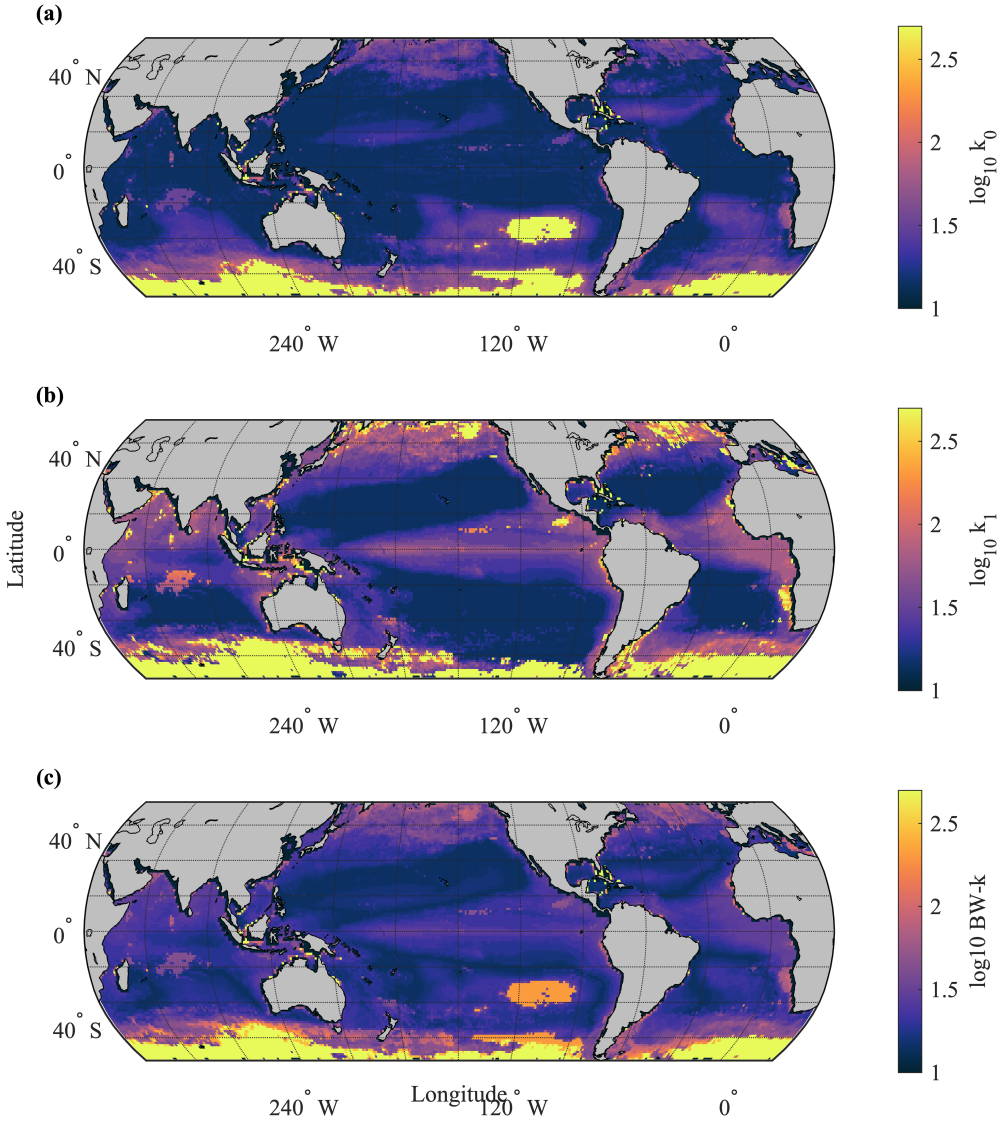

Figure 1. Locally-tuned k values. (a) Microzooplankton half-saturation constants (k_0) estimated using the cost function (Equation 12). b) Mesozooplankton half-saturation constants (k_1) estimated using the cost function. k values are in mgC m^{-3}. c) Biomass-weighted k values (BW-k) which considers the optimal k value for each zooplankton size class and their relative abundance. BW-k reflects the overall grazing dynamics of the entire zooplankton community. The maximum and minimum values on the colourbar represent the maximum/minimum k values sampled in the optimisation.

3.2 Impact of Locally Tuned Grazing Dynamics on Model Skill

Locally-tuned k values improve model skill in comparison to globally homogenous k values (Figure 2). Mean cost (Equation 12) is reduced by 43% in the Local-k scenario, compared to the Global-k scenario. Therefore, the use of locally tuned k values improves

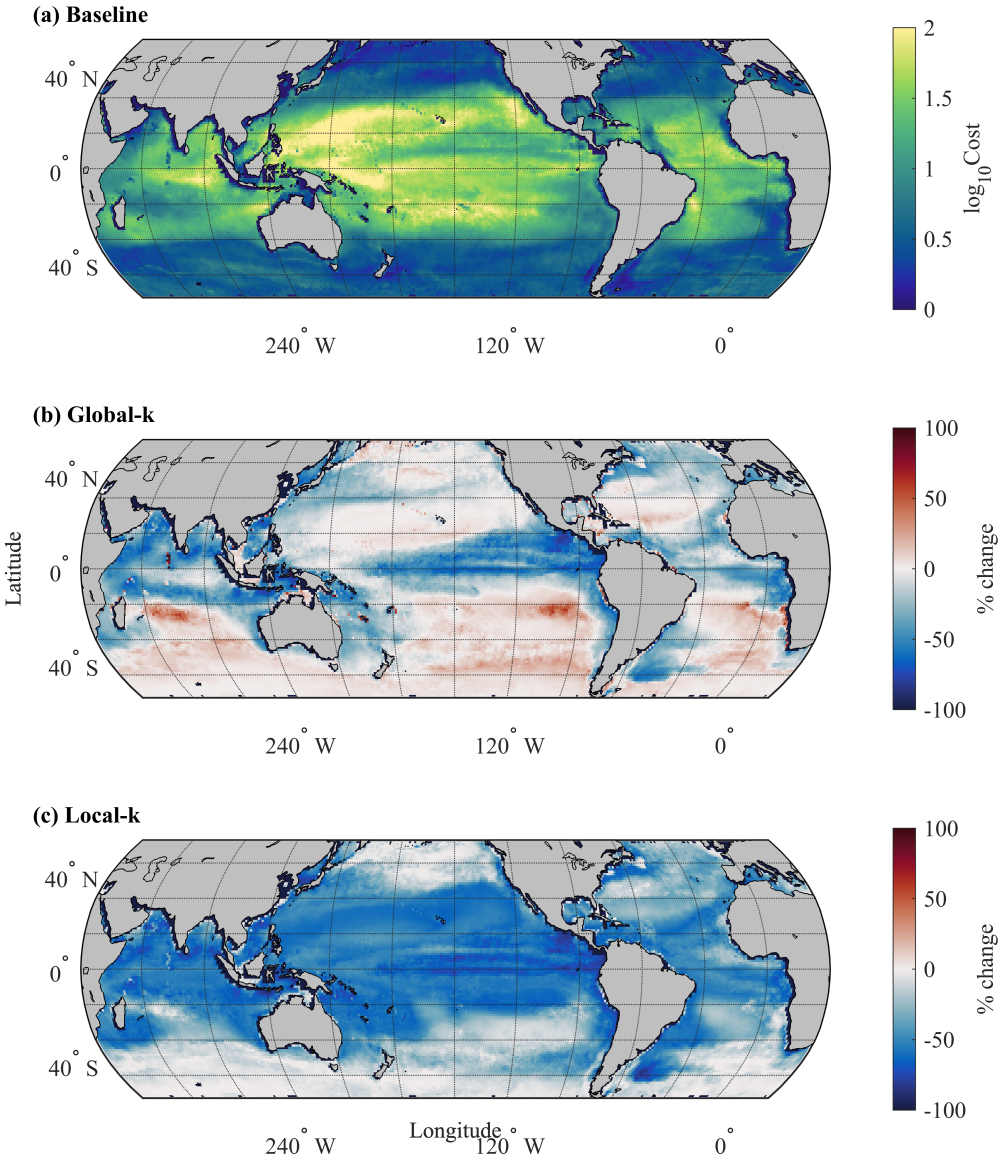

Figure 2. Cost values representing the difference between observations of phytoplankton biomass and the model phytoplankton biomass (Equation 12). a) Cost values from the Baseline model scenario (non-optimised k values). b) Percentage change in cost values in the Global-k scenario compared to the Baseline scenario. c) Percentage change in cost values in the Local-k scenario compared to the Baseline.

the model's ability to reproduce satellite-derived phytoplankton biomass (Figure 3). In comparison, the use of optimised globally homogenous k values (Global-k) has a limited ability (-14%) in reducing model cost from the Baseline scenario. Reduction in cost values due to local tuning is most evident in the tropics and subtropics, particularly productive upwelling regions (Figure 2). Despite improvements, microphytoplankton biomass estimates are the greatest source of error (78%) in the Local-k cost function (Figure S7-8; Table S3).

3.3 Ecosystem Impact

The reproduction of the remotely sensed nanophytoplankton biomass distribution is greatly improved with the implementation of locally tuned k values (Figure 3 & Figure 4a-d). The use of optimised globally homogenous k values (Global-k) improves the reproduction of observed nanophytoplankton but shows little of the regional variability found in observations (Figure 4a & c). This regional variability is only reproduced when locally tuned grazing dynamics are implemented (Figure 4d) highlighting the importance of top-down drivers for this size class. The Local-k model does a good job in estimating global nanophytoplankton biomass with an annual mean ($\pm$ S.D.) of 9.40$\pm$3 mgC m^{-3}, in comparison to 11.89$\pm$6 mgC m^{-3} from satellite-derived estimates (Siegel et al., 2014) (Figure 4a). NPP is 52 and 43 Gt C yr^{-1} for the Local-k and Global-k runs respectively, compared to 87 Gt C yr^{-1} for the non-optimised baseline run (Figure S9).

Microphytoplankton observational distributions are reproduced well in all three model versions showing little difference when locally tuned grazing dynamics are applied (Figure 4e-h), suggesting the distribution for this functional group is determined primarily by realistic bottom-up drivers. However, all three models overestimate biomass in equatorial upwelling areas (Figure 3). In the Local-k model, microphytoplankton has a global mean ($\pm$ S.D.) of 3.05$\pm$3 mgC m^{-3}, compared to 2.62$\pm$5 mgC m^{-3}, from satellite-derived estimates (Siegel et al., 2014) (Figure 4e). In the subtropical oligotrophic gyres, microphytoplankton biomass estimates appear to closely emulate observations, despite higher cost values in this region. This is due to the low biomass in the region, which results in small changes producing large error values with normalisation.

Local-tuning of k values improves zooplankton biomass estimates in comparison to observations (Figure 4i-l & Figure S10). When only optimised homogenous global values are used, global mesozooplankton biomass is underestimated, with a mean ($\pm$ S.D.) of 1.72$\pm$0.81 mgC m^{-3} compared to 5.52$\pm$9 mgC m^{-3} from (Strömberg et al., 2009) (Figure 4i). This is as a result of the very high k value for mesozooplankton (392 mgC m^{-3}), resulting in very low grazing and therefore biomass. In contrast, mean ($\pm$ S.D.) mesozooplankton biomass from the Local-k model is 5.07$\pm$3 mgC m^{-3}. All model versions underestimate mesozooplankton biomass in the higher latitudes of the northern hemisphere. Mean microzooplankton biomass estimates are greatly reduced with the implementation of locally-tuned grazing dynamics, from 29.09$\pm$23 mgC m^{-3} in the Global-k run to 8.85$\pm$11 mgC m^{-3} in the Local-k run (Table 3).

3.4 Impact on Carbon Export

Local tuning of k values decreases mean total carbon export by >17% (Table 3). The magnitude of change depends on the homogenous k values used for comparison (-35.64% in comparison to the Baseline and -17.07% in comparison to the Global-k scenario). Export values are generally high, with a total export flux of 7.19 PgC yr^{-1} for the Local-k scenario and 8.16 Pg C yr^{-1} and 10.94 Pg C yr^{-1} for the Global-k and Baseline scenarios respectively.

The routing of carbon is impacted by the implementation of locally-tuned grazing dynamics (Figure 5). In the Local-k scenario, more carbon is exported as faecal pellets and less as algal aggregates, compared to the Global-k scenario (Table 3). When k values are locally tuned, carbon exported from pellets and aggregates are more similar in magnitude (annual mean of 36.91 and 20.52 mgC m^{-2}d^{-1} respectively) compared to model runs with homogenous k values. In contrast, in both the Baseline and Global-k model runs carbon export is dominated by algal aggregates. Local-tuning of k values also results in increased export (>21%) via vertically migrating zooplankton compared to the Global-k model run (Figure 5, Table 3).

Productive upwelling regions, that are characterised by high carbon export rates, are the regions of greatest change from the local tuning of k values (Figure 5). These patterns

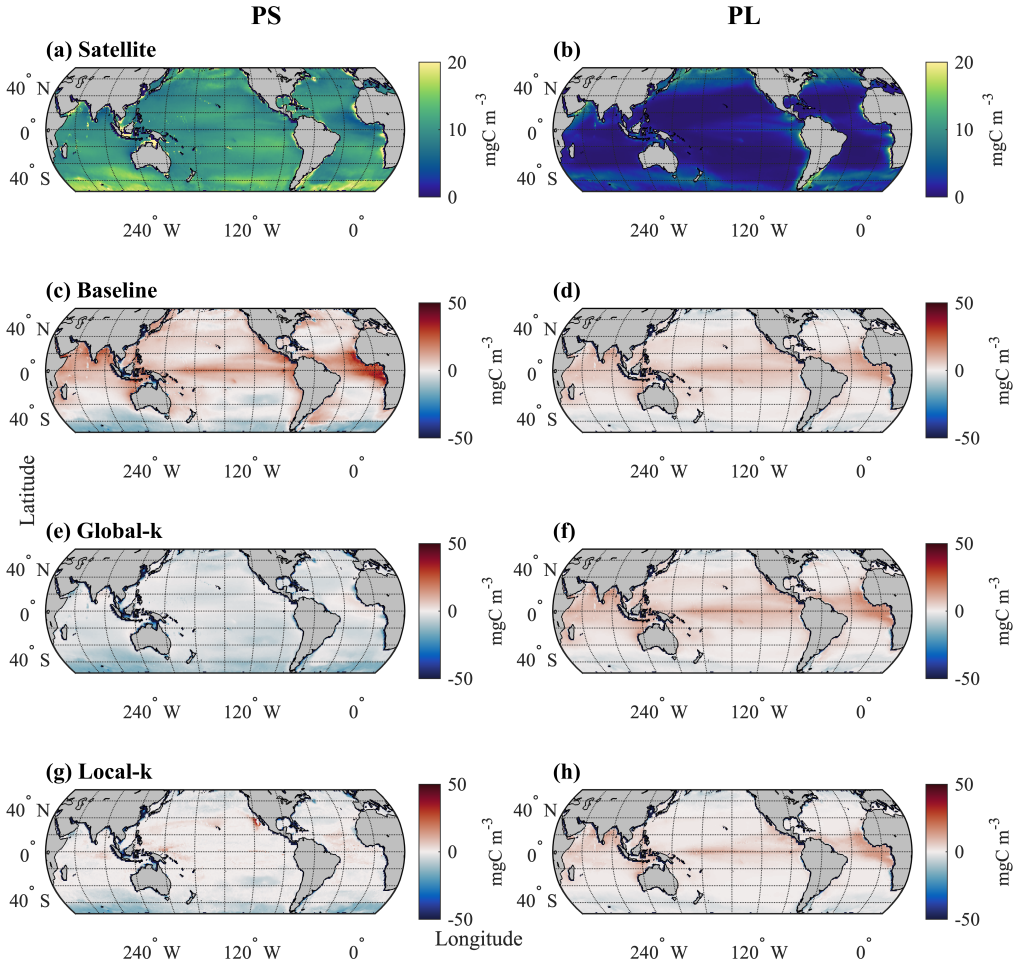

Figure 3. Absolute bias in modelled nanophytoplankton (PS) and microphytoplankton (PL) biomass in comparison to satellite derived biomass (P(i)mod - P(i)obs). Three model scenarios are shown: Baseline (non-optimised k values), Global-k (globally optimised k value) and Local-k (locally tuned k values. Observational phytoplankton biomass values were calculated as per Siegel et al. (2014), using particulate backscattering coefficient data (Behrenfeld et al., 2005; Westberry et al., 2008; Kostadinov et al., 2010; Siegel et al., 2013).

mirror zooplankton grazing rates, for example, changes in fecal export from the euphotic zone (F_{fec}) and DVM-mediated export flux (J_{dvm}) are inversely proportional to those of mesozooplankton grazing. Mesozooplankton grazing on microzooplankton is a greater contributor to carbon flux than grazing on microphytoplankton. In the Local-k model, 80% of mesozooplankton grazing constitutes grazing on microzooplankton ($G_{ZL,ZS}$), however this is decreased from 91% (Baseline-k) and 99% (Global-k) with homogenous k values.

4 Discussion

One of the largest sources of uncertainty in the marine carbon cycle is zooplankton grazing (Rohr et al., 2023a). In this study we used an inverse modelling approach to estimate spatial variation in zooplankton grazing dynamics and explored the subsequent

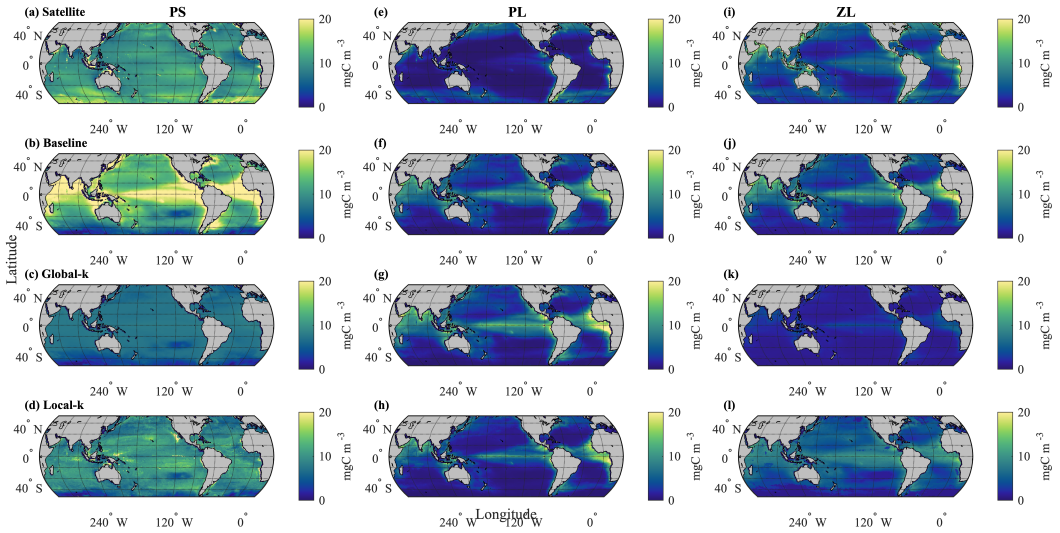

Figure 4. Nanophytoplankton (PS), microphytoplankton (PL) and mesozooplankton (ZL) biomass distributions estimated by the three model scenarios: Baseline, Global-k and Local-k. Satellite-derived biomass distributions are included for reference. a & e are calculated as per Siegel et al. (2014), using particulate backscattering coefficient data (Behrenfeld et al., 2005; Westberry et al., 2008; Kostadinov et al., 2010; Siegel et al., 2013). Satellite-derived mesozooplankton biomass (i) is from Strömberg et al. (2009).

impact of these dynamics on modelling marine ecosystems and carbon export. The focus of this study was the grazing parameter k, which is frequently used in global biogeochemical (BGC) models. We found that local tuning of k results in high variability of inferred grazing dynamics. The local-tuning of k values improved the model's ability to reproduce satellite-derived phytoplankton biomass. Consequently, estimates of mean total carbon export decreased by >17% compared to global tuning, with a greater proportion of export as faecal pellets and less as algal aggregates.

4.1 High Variability of Inferred Grazing Dynamics

Local optimisation suggested high k values were generally associated with eutrophic ocean regions. This is consistent with a study in review (Rohr et al., 2023b) which used an inverse modelling approach to infer high community k values for a single zooplankton group (combining k_0 and k_1) in equatorial upwelling regions and higher latitudes. In equatorial upwelling regions, communities are dominated by suspension-feeding copepods (Steinberg & Landry, 2016), whose slower grazing rates enable diatom blooms to form (Rohr et al., 2023b). In the higher latitudes, higher half-saturation constants reduce grazing pressure on nutrient-limited phytoplankton stocks with slow growth rates, which prevents prey stocks from being fully depleted (Schmoker et al., 2013). Here, higher k values could characterise prey switching events or increased handling time. Christaki et al. (2021) found mesozooplankton in the Southern Ocean preferentially graze on microzooplankton over phytoplankton, due to slow growth rates of the latter.

Generally low k values were estimated in the subtropical oligotrophic gyres, where communities are dominated by faster grazing microzooplankton, in particular pico- and nano-sized flagellates (Calbet & Calbet, 2008). Anomalous high k_0 values inferred in the hyper-oligotrophic South Pacific gyre (Ras et al., 2007) are in disagreement to the study by Rohr et al. (2023b) and coincide with an underestimation of NPP, nanophytoplankton

Table 3. Comparison of mean global carbon export estimates from the three model scenarios. NPP = Net Primary Productivity. F_{alg} = Euphotic export flux of algal aggregates. F_{fec} = Euphotic export flux of faecal pellets. J_{dvm} = DVM-mediated export flux. G_{ZL} = Mesozooplankton grazing rate on all prey types. G_{ZS} = Microzooplankton grazing rate on all prey types. $G_{ZL,PL}$ = Mesozooplankton grazing on microphytoplankton. $G_{ZL,ZS}$ = Mesozooplankton grazing on microzooplankton. PS = Nanophytoplankton biomass. PL = Microphytoplankton biomass. ZS = Microzooplankton biomass. ZL = Mesozooplankton biomass. DER = DVM export ratio. DRR = DVM respiration ratio.

	Baseline		Global-k		Local-k	
	Mean	S.D.	Mean	S.D.	Mean	S.D.
Export Flux (mgC $m^{-2}d^{-1}$)	93.48	127.46	69.44	107.14	61.74	88.32
NPP (mgC $m^{-2}d^{-1}$)	752.18	715.79	379.36	283.08	459.04	291.66
Export Ratio	0.09	0.05	0.12	0.10	0.10	0.08
PS (mgC m^{-3})	13.95	6.39	6.65	1.49	9.40	2.86
PL (mgC m^{-3})	4.04	3.52	4.38	4.03	3.05	3.32
ZS (mgC m^{-3})	16.69	11.59	29.09	29.91	8.85	11.21
ZL (mgC m^{-3})	4.66	3.62	1.72	0.81	5.07	2.70
G_{ZS} (mgC $m^{-3}d^{-1}$)	6.33	8.08	3.00	2.63	3.73	3.38
G_{ZL} (mgC $m^{-3}d^{-1}$)	4.66	3.62	1.72	0.81	5.07	2.70
$G_{ZL,PL}$ (mgC $m^{-3}d^{-1}$)	0.11	0.25	$1.7x10^{-3}$	$4.1x10^{-3}$	0.21	0.31
$G_{ZL,ZS}$ (mgC $m^{-3}d^{-1}$)	1.12	1.91	0.06	0.12	0.88	0.84
F_{alg} (mgC $m^{-2}d^{-1}$)	68.54	88.19	68.28	104.98	36.91	72.32
F_{fec} (mgC $m^{-2}d^{-1}$)	20.70	33.14	0.97	1.84	20.52	18.76
J_{dvm} (mgC $m^{-2}d^{-1}$)	4.24	6.53	0.20	0.36	4.31	3.65
DER	0.03	0.02	$3.2x10^{-3}$	$2.3x10^{-3}$	0.10	0.06
DRR	0.03	0.02	$2.7x10^{-3}$	$2.0x10^{-3}$	0.11	0.06

biomass and near-zero growth rates. This suggests that in this region, nanophytoplankton growth rates used to force the model may be too low. Growth rates are derived from observed NPP, which is divided by the greater of euphotic and mixed layer depth. The South Pacific gyre is characterised by a deep euphotic layer, which may have produced unrealistically low growth rates and anomalous k values for this size class. In addition, the lack of explicit representation of temperature within the model may affect growth and grazing rates in these extreme environments. The 1P1Z 3D model in Rohr et al. (2023b) uses modelled rather than observationally derived bottom-up controls which may negate these issues.

In this study, mesozooplankton showed on average, higher k values, and therefore slower prey capture times. This is consistent with ecological understanding (Barton et al., 2013). As the maximum grazing rate, g, was held constant across the model domain, variation in the k value represents variation in the prey capture rate, rather than consumption (Rohr et al., 2022). For both size classes, average half-saturation constants were in the lower quartile of empirical values (Rohr et al., 2022; Hansen et al., 1997; Hirst & Bunker, 2003). However, empirical estimates are from laboratory measurements of samples collected from a very narrow range of locations, with the majority from coastal regions in the northern hemisphere (e.g. fjords in Norway, coastal USA and UK, Japan) and none representing the open ocean (Hansen et al., 1997; Hirst & Bunker, 2003). These are also of individual species and are unlikely to be representative of the community mean values estimated here for each 1 degree grid cell (Rohr et al., 2022).

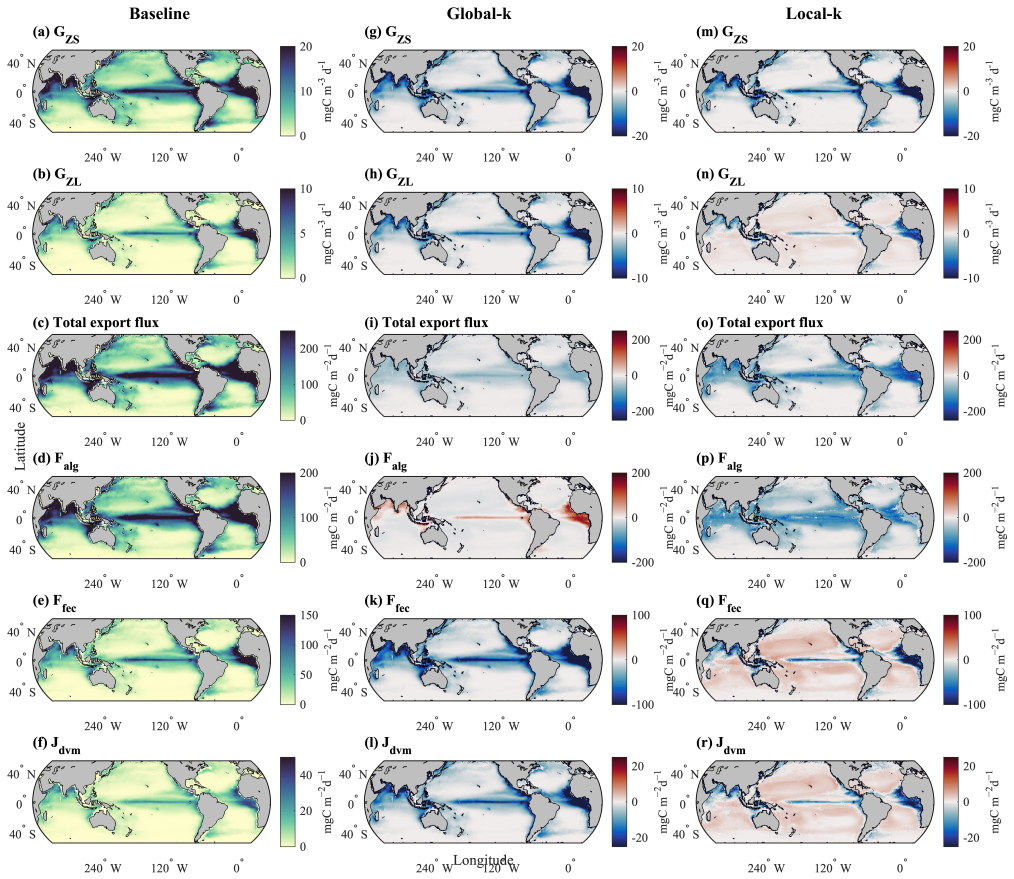

Figure 5. Changes in carbon export due to grazing parameterisation. Three model runs are presented: Baseline, Global-k and Local-k. The outputs from the Baseline run are presented in plots a-f. Plots g-l show the absolute change when changing the model input from the baseline run (non-optimised k values) to the Global-k run (globally optimised k values). Plots m-r show the absolute change when changing the model input from the Global-k run (globally optimised k values) to the Local-k run (locally tuned k values). F_{alg} = Euphotic export flux of algal aggregates. F_{fec} = Euphotic export flux of faecal pellets. J_{dvm} = DVM-mediated export flux. G_{ZL} = Mesozooplankton grazing rate on all prey types. G_{ZS} = Microzooplankton grazing rate on all prey types.

Locally-tuned k values produced global distributions of grazing rates (G_i) that are consistent with other studies (Siegel et al., 2014; Archibald et al., 2019). Archibald et al. (2019) used satellite-derived estimates of Net Primary Productivity (NPP) and phytoplankton biomass to predict global grazing rates. Mean G_{ZS} was 4.17 mgC $m^{-3}d^{-1}$ and mean $G_{ZL,PL}$ was 0.98 mgC$m^{-3}d^{-1}$ in Archibald et al. (2019). These represent grazing mortalities from satellite observations on phytoplankton, so include grazing losses by other groups not considered here (e.g. mesozooplankton grazing on nanophytoplankton). However, the Local-k model improves the reproduction of these observationally derived grazing rates in comparison to globally homogenous k values (Table 3), with the potential to help address the uncertainty in global zooplankton grazing dynamics.

4.2 Implications of Improved Model Skill for Future Studies

With potential to improve model skill, the local optimisation of grazing dynamics could be advisable in future BGC modelling studies. This study shows that the competition generated by two zooplankton functional types isn't sufficient to emulate the global variability in grazing suggested by the locally tuning k values. Other models currently emulate this dynamical variability using different methods, such as increased numbers of plankton functional groups (PFTs) (e.g. Dutkiewicz et al. (2021), prey switching (e.g. Anderson et al. (2010)), or prey preferences (e.g. Aumont et al. (2015)). In this study, four PFTs were used, in line with several modelling studies (e.g. Siegel et al. (2014)), however, this groups together species with different functional traits, with different geographic distributions (Barton et al., 2013). Gelatinous salps, for example, graze preferentially on nanophytoplankton, which leads to their prevalence in subtropical oligotrophic gyres (Barton et al., 2013). By explicitly representing more PFTs and their prey preferences, some of the impact of locally-tuning k values may be reduced. A study by Le Quéré et al. (2016) showed that the explicit representation of krill in the Southern Ocean improved model skill in reproducing zooplankton dynamics. However, increasing the number of PFTs is computationally costly and unlikely to encompass the full extent of physiological and behavioural diversity found within the plankton community The global distributions of the grazing parameter k, produced in this study, could provide a platform for varying zooplankton grazing parameters in larger, more complicated BGC models, with environmental conditions. If the variability in local tuned k values correlates with key environmental variables, then grazing dynamics could be implemented as a function of covariates. This could improve model skill in comparison to the use of globally homogenous k values, whilst remaining computationally effective. This work is beyond the scope of this study but is an area for further work.

4.3 Reducing Uncertainty in Modelling Zooplankton

Large uncertainty exists in quantifying zooplankton biomass (Petrik et al., 2022), however the use of locally tuned k values improves the models ability to reproduce observational estimates. The observed mean ($\pm$S.D.) biomass of mesozooplankton is estimated as 5.9$\pm$10.6 mgC m^{-3} by Buitenhuis et al. (2013); Moriarty and O'Brien (2013), which compares to 5.07 $\pm$2.7 mgC m^{-3} in the Local-k model scenario. In contrast, optimised globally homogenous k values worsen the model's ability to reproduce observational mesozooplankton biomass in comparison to the Baseline scenario (Table 3). This highlights a potential limitation of global optimisation of grazing dynamics when only two zooplankton functional groups are used. This also suggests a possible reason why several BGC models underestimate mean global mesozooplankton biomass by a similar magnitude (Figure S10) (Aumont et al., 2015; Lovato et al., 2022). In addition, mean global microzooplankton estimates from the Global-k scenario are much greater than observations by Buitenhuis et al. (2013), where biomass is estimated to have a mean of 9.3$\pm$17.1 mgC m^{-3} and a median of 3.1 mgC m^{-3}. These limitations occur despite improved model skill at reproducing the magnitude and distribution of satellite-derived phytoplankton. Local-k mean global biomass for microphytoplankton is within the range of estimates by Buitenhuis et al. (2013)(Table 3).

4.4 Implications for Predicting Carbon Export under a Changing Climate

This study shows large variability in carbon export estimates driven by inferred grazing dynamics. There is a high degree of uncertainty in global export flux estimates, which vary between 5-12 PgC yr^{-1} (Siegel et al., 2022). Locally tuning grazing dynamics modifies carbon export estimates by >17% to coincide with this range (7.19 PgC yr^{-1}). The Global-k scenario estimates high carbon export, despite underestimating mesozooplankton biomass and therefore fecal export. This is due to a large proportion of algal aggregates. The substantial influence of this one model component on carbon export highlights one possible cause for uncertainty in carbon sequestration estimates (Laufkötter et al., 2016). It is vital to reduce this uncertainty when modelling under different climate scenarios.

Algal and fecal estimates were closer to contributing equally to carbon export (as found within previous studies (Stock et al., 2014; Steinberg & Landry, 2016)) when grazing dynamics were locally optimised. The relationship between algal aggregates and faecal export highlights the balance between natural and grazing mortalities within BGC models, as the amount of biomass available for aggregates from mortality rates is impacted by grazing. The proportion of faecal versus algal export is determined by the zooplankton species present and their grazing dynamics (Steinberg & Landry, 2016). Local tuning of grazing dynamics therefore has important consequences for climate models as the impact of climate change on plankton communities differs between species, trophic levels and geographic location (Cael et al., 2021), further influencing these two routes of carbon export.

The modelled distribution of carbon export corresponds to estimates by Stock et al. (2020), with coastal upwelling areas experiencing the greatest change from the local tuning of k. These areas produce the highest export rates due to more efficient diatom-copepod food chains (Schmoker et al., 2013). However, the fast growth rates of diatoms makes them more susceptible to abrupt changes over the 21st Century in response to climate change (Cael et al., 2021). It is therefore vital to decrease uncertainty in grazing and export estimates in these areas. The subtropical oligotrophic gyres and the Southern Ocean are areas of lower carbon export due to the presence of smaller phytoplankton species which are lighter, sinking less carbon into the ocean interior (Murphy et al., 2021; Schmoker et al., 2013; Calbet & Landry, 2004). The highest flux estimates in the Southern Ocean occur closer to the Antarctic shelf edge, predominantly during summer months (Stock et al., 2020). However the polar extremes are out of the scope of this study due to the limitations of satellite observations in these areas (Siegel et al., 2014), which is a common issue with many plankton models (Cael et al., 2021; Dutkiewicz et al., 2021).

4.5 Limitations

There are several limitations of this modelling study. Firstly, non-k parameters are held constant across the model domain, when in reality they are likely to vary in space and time. If these other parameters were tuned, the non-optimised (Baseline scenario) estimate of NPP may be reduced to coincide with the observed range (45-60 GtC yr^{-1}) (Westberry et al., 2008; Le Quéré et al., 2016) alongside the two optimised model scenarios. $G_{Zl,PL}$ and $G_{Zl,ZS}$ also use the same k value, which obscures whether changes in k_1 are biased to improve microphytoplankton estimates or nanophytoplankton estimates (via microzooplankton) during the cost analysis. This may contribute to the overestimation of microphytoplankton in all model runs. Secondly, grazing formulas are based on the Holling Type III functional response, however there is a lack of consensus within the modelling community about the most suitable functional response. Anderson et al. (2010) found that the use of different grazing formulations caused large variations in biomass, with diatoms most greatly affected. This resulted in carbon export predictions varying by as much as 25%. Thirdly, within the centre of the oligotrophic gyres, microzooplankton were characterised by less efficient prey capture rates compared to mesozooplankton (Figure S5), however prey capture efficiency should decline with size (Rohr et al., 2022; Hansen et al., 1997). This highlights a possible limitation of the model, potentially the functional groups used or model parameters. In this study, the same maximum grazing rate was used for both size classes, so prey capture efficiency is dominated by the half-saturation constant, or capture rate. In oligotrophic regions, smaller plankton dominate, so prey capture efficiencies for microzooplankton are more likely to be driven by consumption rather than capture rates, suggesting higher maximum grazing rates are needed to represent realistic capture efficiencies in these environments. Fourthly, CbPMv2 was selected as the NPP forcing variable for consistency with Archibald et al. (2019), however other NPP models such as the The Carbon, Absorption, and Fluorescence Euphotic-resolving (CAFE) (Silsbe et al., 2016) have been found to be more realistic, with consequences for carbon export (Bisson et al., 2018). Finally, the carbon export model does have several limitations which are discussed in detail in Archibald et al. (2019). In particular, the model is very sensitive to three parameters – $ffec$, $fmet$

and *pdvm*, however these parameters remain unchanged to enable comparisons. The model also doesn't include small fecal pellets produced by microzooplankton in carbon export estimates as they are assumed to be retained in the euphotic zone. However, some studies suggest fecal export by this size class could contribute a significant portion of export flux, particularly in the subtropical oligotrophic gyres Bisson et al. (2020).

4.6 Future Considerations

The simplification of the coupled ecosystem-carbon export model means the results of this study should be considered as an example of an ecosystem model with and without spatially varying k values. Here, we have shown that highly spatially heterogeneous grazing dynamics are required to reproduced observed biomass when forced with observed bottom-up controls. This heterogeneity exceeds what is achievable from the explicit competition between two zooplankton functional types and has profound implications for the routing and magnitude of carbon export. Future models, particularly those concerned with ecosystem dynamics, high trophic levels and carbon export must reconcile with the possibility that even two zooplankton groups are insufficient to capture the true variability in top-down controls across the globe. More realistic representation of the global variability in zooplankton grazing dynamics may help shed light on the uncertainty in carbon export estimates under future climate scenarios.

5 Open Research

Climatologies used here are presented in detail in Siegel et al. (2014). CbPMv2 (Westberry et al., 2008) Net Primary Productivity, particulate backscatter (used to derive phytoplankton carbon biomass) and mixed layer depth data can be sourced from: http://orca.science.oregonstate.edu/npp_ products.php. World Ocean Atlas temperature and oxygen data used in the Archibald et al. (2019) carbon export model can be found at: (https://coastwatch.pfeg.noaa.gov/erddap/index.html).

Acknowledgments

SM acknowledges support from the Natural Environment Research Council through the C-CLEAR Doctoral Training Partnership [grant number NE/S007164/1]. CMP acknowledges support from NOAA grants NA20OAR4310438, NA20OAR4310441 and NA20OAR4310442. TR is the recipient of an Australian Research Council Discovery Early Career Award (project number DE240100115) funded by the Australian Government. TR received grant funding from the Australian Government as part of the Antarctic Science Collaboration Initiative program. The authors would like to thank Dr. Kevin Archibald and Prof. David Siegel for providing data and code from their previous publications (Siegel et al., 2014; Archibald et al., 2019). The authors declare no conflicts of interest.

References

Anderson, T. R., Gentleman, W. C., & Sinha, B. (2010, 10). Influence of grazing formulations on the emergent properties of a complex ecosystem model in a global ocean general circulation model. *Progress in Oceanography*, *87*, 201-213. doi: 10.1016/J.POCEAN.2010.06.003

Anderson, T. R., Gentleman, W. C., & Yool, A. (2015). Empower-1.0: an efficient model of planktonic ecosystems written in r. *Geosci. Model Dev*, *8*, 2231-2262. Retrieved from `www.geosci-model-dev.net/8/2231/2015/` doi: 10.5194/gmd-8-2231-2015

Archibald, K. M., Siegel, D. A., & Doney, S. C. (2019). Modeling the impact of zooplankton diel vertical migration on the carbon export flux of the biological pump. *Global Biogeochemical Cycles*, *33*, 181-199. Retrieved from `https://doi.org/10.1029/`

2018GB005983 doi: 10.1029/2018GB005983

Aumont, O., Ethé, C., Tagliabue, A., Bopp, L., & Gehlen, M. (2015). Pisces-v2: an ocean biogeochemical model for carbon and ecosystem studies. *Geosci. Model Dev*, *8*, 2465-2513. Retrieved from www.geosci-model-dev.net/8/2465/2015/ doi: 10.5194/gmd-8-2465-2015

Barton, A. D., Pershing, A. J., Litchman, E., Record, N. R., Edwards, K. F., Finkel, Z. V., ... Ward, B. A. (2013, 4). The biogeography of marine plankton traits. *Ecology letters*, *16*, 522-534. Retrieved from https://pubmed.ncbi.nlm.nih.gov/23360597/ doi: 10.1111/ELE.12063

Behrenfeld, M. J., Boss, E., Siegel, D. A., Shea, D. M., Behrenfeld, M. J., Boss, E., ... Shea, D. M. (2005, 3). Carbon-based ocean productivity and phytoplankton physiology from space. *Global Biogeochemical Cycles*, *19*, 1-14. Retrieved from https://onlinelibrary.wiley.com/doi/full/10.1029/2004GB002299https://onlinelibrary.wiley.com/doi/abs/10.1029/2004GB002299https://agupubs.onlinelibrary.wiley.com/doi/10.1029/2004GB002299 doi: 10.1029/2004GB002299

Bisson, K., Siegel, D. A., & DeVries, T. (2020, 7). Diagnosing mechanisms of ocean carbon export in a satellite-based food web model. *Frontiers in Marine Science*, *7*, 518850. doi: 10.3389/FMARS.2020.00505/BIBTEX

Bisson, K., Siegel, D. A., DeVries, T., Cael, B. B., & Buesseler, K. O. (2018, 9). How data set characteristics influence ocean carbon export models. *Global Biogeochemical Cycles*, *32*, 1312-1328. doi: 10.1029/2018GB005934

Boyd, P. W. (2015). Toward quantifying the response of the oceans' biological pump to climate change. *Frontiers in Marine Science*, *2*, 77. doi: 10.3389/FMARS.2015.00077/BIBTEX

Buitenhuis, E. T., Vogt, M., Moriarty, R., Bednaršek, N., Doney, S. C., Leblanc, K., ... Swan, C. (2013). Earth system science data maredat: towards a world atlas of marine ecosystem data. *Earth Syst. Sci. Data*, *5*, 227-239. Retrieved from www.earth-syst-sci-data.net/5/227/2013/Microzooplanktondatabase:doi:10.1594/PANGAEA.779970AllMAREDATdatabases:http://www.pangaea.de/search?&q=maredat doi: 10.5194/essd-5-227-2013

Cael, B. B., Dutkiewicz, S., & Henson, S. (2021, 10). Abrupt shifts in 21st-century plankton communities. *Science Advances*, *7*, 8593-8622. Retrieved from https://www.science.org/doi/abs/10.1126/sciadv.abf8593 doi: 10.1126/SCIADV.ABF8593/SUPPL_FILE/SCIADV.ABF8593_SM.PDF

Calbet, A., & Calbet, A. (2008, 4). The trophic roles of microzooplankton in marine systems. *ICES Journal of Marine Science*, *65*, 325-331. Retrieved from https://academic.oup.com/icesjms/article/65/3/325/786057 doi: 10.1093/ICESJMS/FSN013

Calbet, A., & Landry, M. R. (2004). Phytoplankton growth, microzooplankton grazing, and carbon cycling in marine systems. *Limnol. Oceanogr*, *49*, 51-57. Retrieved from https://aslopubs.onlinelibrary.wiley.com/doi/10.4319/lo.2004.49.1.0051 doi: 10.4319/lo.2004.49.1.0051

Christaki, U., Skouroliakou, I. D., Delegrange, A., Irion, S., Courcot, L., Jardillier, L., & Sassenhagen, I. (2021, 7). Microzooplankton diversity and potential role in carbon cycling of contrasting southern ocean productivity regimes. *Journal of Marine Systems*, *219*, 103531. doi: 10.1016/J.JMARSYS.2021.103531

DeVries, T. (2022, 10). The ocean carbon cycle. *Annual Review of Environment and Resources*, *47*, 317-341. Retrieved from https://www.annualreviews.org/doi/abs/10.1146/annurev-environ-120920-111307 doi: 10.1146/ANNUREV-ENVIRON-120920-111307

Dutkiewicz, S., Boyd, P. W., & Riebesell, U. (2021, 3). Exploring biogeochemical and ecological redundancy in phytoplankton communities in the global ocean. *Global Change Biology*, *27*, 1196-1213. Retrieved from https://onlinelibrary.wiley.com/doi/full/10.1111/gcb.15493https://onlinelibrary.wiley.com/doi/abs/10.1111/gcb.15493https://onlinelibrary.wiley.com/doi/10.1111/gcb.15493 doi:

10.1111/GCB.15493

Evans, G. T., & Parslow, J. S. (1985). A model of annual plankton cycles. *Biological oceanography*, *3*, 327-347. Retrieved from https://www.tandfonline.com/action/journalInformation?journalCode=tboc20 doi: 10.1080/01965581.1985.10749478

Friedlingstein, P., Jones, M. W., O'Sullivan, M., Andrew, R. M., Bakker, D. C. E., Hauck, J., ... Zeng, J. (2022, 4). Global carbon budget 2021. *Earth System Science Data*, *14*, 1917–2005. Retrieved from https://research-portal.uea.ac.uk/en/publications/global-carbon-budget-2021 doi: 10.5194/ESSD-2021-386

Gentleman, W., Leising, A., Frost, B., Strom, S., & Murray, J. (2003, 11). Functional responses for zooplankton feeding on multiple resources: a review of assumptions and biological dynamics. *Deep Sea Research Part II: Topical Studies in Oceanography*, *50*, 2847-2875. doi: 10.1016/J.DSR2.2003.07.001

Gentleman, W., & Neuheimer, A. B. (2008). Functional responses and ecosystem dynamics: how clearance rates explain the influence of satiation, food-limitation and acclimation. *Journal of Plankton Research*, *30*, 1215-1231. Retrieved from www.plankt.oxfordjournals.org doi: 10.1093/plankt/fbn078

Hansen, P. J., Bjørnsen, P. K., & Hansen, B. W. (1997, 6). Zooplankton grazing and growth: Scaling within the 2-2,-m body size range. *Limnology and Oceanography*, *42*, 687-704. Retrieved from https://onlinelibrary.wiley.com/doi/full/10.4319/lo.1997.42.4.0687https://onlinelibrary.wiley.com/doi/abs/10.4319/lo.1997.42.4.0687https://aslopubs.onlinelibrary.wiley.com/doi/10.4319/lo.1997.42.4.0687 doi: 10.4319/LO.1997.42.4.0687

Hirst, A. G., & Bunker, A. J. (2003). Growth of marine planktonic copepods: Global rates and patterns in relation to chlorophyll a, temperature, and body weight. *Limnol. Oceanogr*, *48*. Retrieved from https://aslopubs.onlinelibrary.wiley.com/doi/10.4319/lo.2003.48.5.1988 doi: 10.4319/lo.2003.48.5.1988

Hoegh-Guldberg, O., & Bruno, J. F. (2010, 6). The impact of climate change on the world's marine ecosystems. *Science*, *328*, 1523-1528. Retrieved from https://www.science.org/doi/10.1126/science.1189930 doi: 10.1126/SCIENCE.1189930/ASSET/F23D4D51-3B99-42AD-A2B7-C0B9B167A930/ASSETS/GRAPHIC/328_1523_B1.JPEG

Holling, C. S. (1959). The components of predation as revealed by a study of small-mammal predation of the european pine sawfly. *The Canadian Entomologist*, *91*, 293-320. doi: 10.4039/ENT91293-5

Kearney, K. A., Bograd, S. J., Drenkard, E., Gomez, F. A., Haltuch, M., Hermann, A. J., ... Woodworth-Jefcoats, P. A. (2021, 8). *Using global-scale earth system models for regional fisheries applications* (Vol. 8). Frontiers Media S.A. doi: 10.3389/fmars.2021.622206

Kostadinov, T. S., Siegel, D. A., & Maritorena, S. (2010). Global variability of phytoplankton functional types from space: Assessment via the particle size distribution. *Biogeosciences*, *7*, 3239-3257. doi: 10.5194/BG-7-3239-2010

Laufkötter, C., Vogt, M., Gruber, N., Aumont, O., Bopp, L., Doney, S. C., ... Völker, C. (2016, 7). Projected decreases in future marine export production: The role of the carbon flux through the upper ocean ecosystem. *Biogeosciences*, *13*, 4023-4047. doi: 10.5194/BG-13-4023-2016

Le Quéré, C., Buitenhuis, E. T., Moriarty, R., Alvain, S., Aumont, O., Bopp, L., ... Vallina, S. M. (2016). Role of zooplankton dynamics for southern ocean phytoplankton biomass and global biogeochemical cycles. *Biogeosciences*, *13*, 4111-4133. Retrieved from www.biogeosciences.net/13/4111/2016/ doi: 10.5194/bg-13-4111-2016

Lovato, T., Peano, D., Butenschön, M., Materia, S., Iovino, D., Scoccimarro, E., ... Navarra, A. (2022, 3). Cmip6 simulations with the cmcc earth system model (cmcc-esm2). *Journal of Advances in Modeling Earth Systems*, *14*. Retrieved from https://onlinelibrary.wiley.com/doi/full/10.1029/2021MS002814https://onlinelibrary.wiley.com/doi/abs/10.1029/2021MS002814https://agupubs.onlinelibrary.wiley.com/doi/10.1029/

2021MS002814 doi: 10.1029/2021MS002814

McClain, C. R. (2009, 3). A decade of satellite ocean color observations. *Annual Review of Marine Science*, *1*, 19-42. Retrieved from https://www.annualreviews.org/doi/abs/10.1146/annurev.marine.010908.163650 doi: 10.1146/ANNUREV.MARINE.010908.163650

Moriarty, R., & O'Brien, T. D. (2013, 2). Distribution of mesozooplankton biomass in the global ocean. *Earth System Science Data*, *5*, 45-55. doi: 10.5194/ESSD-5-45-2013

Murphy, E. J., Johnston, N. M., Hofmann, E. E., Phillips, R. A., Jackson, J. A., Constable, A. J., ... Xavier, J. C. (2021, 8). Global connectivity of southern ocean ecosystems. *Frontiers in Ecology and Evolution*, *9*. doi: 10.3389/fevo.2021.624451

Petrik, C. M., Luo, J. Y., Heneghan, R. F., Everett, J. D., Harrison, C. S., & Richardson, A. J. (2022, 11). Assessment and constraint of mesozooplankton in cmip6 earth system models. *Global Biogeochemical Cycles*, *36*. doi: 10.1029/2022GB007367

Ras, J., Claustre, H., & Uitz, J. (2007, 10). Spatial variability of phytoplankton pigment distributions in the subtropical south pacific ocean: comparison between in situ and predicted data. *Biogeosciences Discussions*, *4*, 3409-3451. Retrieved from https://hal.science/hal-00330270https://hal.science/hal-00330270/document

Rohr, T., Anthony, J. R., Lenton, A., Chamberlain, M. A., & Shadwick, E. H. (2023a). Zooplankton grazing is the largest source of uncertainty for marine carbon cycling in cmip6 models. *Nature Communications Earth Envrionment*, *4*.

Rohr, T., Richardson, A., Lenton, A., Chamberlain, M., & Shadwick, E. (2023b). The global distribution and drivers of grazing dynamics estimated from inverse modelling. *Nature Communications Earth Envrionment*, *4*.

Rohr, T., Richardson, A. J., Lenton, A., & Shadwick, E. (2022, 11). Recommendations for the formulation of grazing in marine biogeochemical and ecosystem models. *Progress in Oceanography*, *208*. doi: 10.1016/J.POCEAN.2022.102878

Schmoker, C., Hernández-León, S., & Calbet, A. (2013, 7). Microzooplankton grazing in the oceans: impacts, data variability, knowledge gaps and future directions. *Journal of Plankton Research*, *35*, 691-706. Retrieved from https://academic.oup.com/plankt/article/35/4/691/1525584 doi: 10.1093/PLANKT/FBT023

Sieburth, J. M. N., Smetacek, V., & Lenz, J. (1978, 11). Pelagic ecosystem structure: Heterotrophic compartments of the plankton and their relationship to plankton size fractions 1. *Limnology and Oceanography*, *23*, 1256-1263. Retrieved from https://onlinelibrary.wiley.com/doi/full/10.4319/lo.1978.23.6.1256https://onlinelibrary.wiley.com/doi/abs/10.4319/lo.1978.23.6.1256https://aslopubs.onlinelibrary.wiley.com/doi/10.4319/lo.1978.23.6.1256 doi: 10.4319/LO.1978.23.6.1256

Siegel, D. A., Behrenfeld, M. J., Maritorena, S., McClain, C. R., Antoine, D., Bailey, S. W., ... Yoder, J. A. (2013, 8). Regional to global assessments of phytoplankton dynamics from the seawifs mission. *Remote Sensing of Environment*, *135*, 77-91. doi: 10.1016/J.RSE.2013.03.025

Siegel, D. A., Buesseler, K. O., Doney, S. C., Sailley, S. F., Behrenfeld, M. J., & Boyd, P. W. (2014, 3). Global assessment of ocean carbon export by combining satellite observations and food-web models. *Global Biogeochemical Cycles*, *28*, 181-196. Retrieved from https://onlinelibrary.wiley.com/doi/full/10.1002/2013GB004743https://onlinelibrary.wiley.com/doi/abs/10.1002/2013GB004743https://agupubs.onlinelibrary.wiley.com/doi/10.1002/2013GB004743 doi: 10.1002/2013GB004743

Siegel, D. A., DeVries, T., Cetinić, I., & Bisson, K. M. (2022, 9). Quantifying the ocean's biological pump and its carbon cycle impacts on global scales. *Annual review of marine science*, *15*, 329-356. Retrieved from https://www.annualreviews.org/doi/abs/10.1146/annurev-marine-040722-115226 doi: 10.1146/ANNUREV-MARINE-040722-115226

Silsbe, G. M., Behrenfeld, M. J., Halsey, K. H., Milligan, A. J., & Westberry, T. K. (2016, 12). The cafe model: A net production model for global ocean phy-

toplankton. *Global Biogeochemical Cycles*, *30*, 1756-1777. Retrieved from https://onlinelibrary.wiley.com/doi/full/10.1002/2016GB005521https://onlinelibrary.wiley.com/doi/abs/10.1002/2016GB005521https://agupubs.onlinelibrary.wiley.com/doi/10.1002/2016GB005521 doi: 10.1002/2016GB005521

Steinberg, D. K., & Landry, M. R. (2016). Zooplankton and the ocean carbon cycle. *Annual review of marine science*, *9*, 413-444. Retrieved from www.annualreviews.org doi: 10.1146/annurev-marine-010814-015924

Stock, C. A., & Dunne, J. (2010, 1). Controls on the ratio of mesozooplankton production to primary production in marine ecosystems. *Deep-Sea Research Part I: Oceanographic Research Papers*, *57*, 95-112. doi: 10.1016/j.dsr.2009.10.006

Stock, C. A., Dunne, J. P., Fan, S., Ginoux, P., John, J., Krasting, J. P., ... Zadeh, N. (2020, 10). Ocean biogeochemistry in gfdl's earth system model 4.1 and its response to increasing atmospheric co2. *Journal of Advances in Modeling Earth Systems*, *12*. Retrieved from https://onlinelibrary.wiley.com/doi/full/10.1029/2019MS002043https://onlinelibrary.wiley.com/doi/abs/10.1029/2019MS002043https://agupubs.onlinelibrary.wiley.com/doi/10.1029/2019MS002043 doi: 10.1029/2019MS002043

Stock, C. A., Dunne, J. P., & John, J. G. (2014, 1). Global-scale carbon and energy flows through the marine planktonic food web: An analysis with a coupled physical–biological model. *Progress in Oceanography*, *120*, 1-28. doi: 10.1016/J.POCEAN.2013.07.001

Stow, C. A., Jolliff, J., McGillicuddy, D. J., Doney, S. C., Allen, J. I., Friedrichs, M. A., ... Wallhead, P. (2009, 2). Skill assessment for coupled biological/physical models of marine systems. *Journal of Marine Systems*, *76*, 4-15. doi: 10.1016/J.JMARSYS.2008.03.011

Strömberg, K. H., Smyth, T. J., Allen, J. I., Pitois, S., & O'Brien, T. D. (2009, 8). Estimation of global zooplankton biomass from satellite ocean colour. *Journal of Marine Systems*, *78*, 18-27. doi: 10.1016/J.JMARSYS.2009.02.004

Turner, J. T. (2015). Zooplankton fecal pellets, marine snow, phytodetritus and the ocean's biological pump. *Progress in Oceanography*, *130*, 205-248. Retrieved from http://dx.doi.org/10.1016/j.pocean.2014.08.005 doi: 10.1016/j.pocean.2014.08.005

Vallina, S. M., Ward, B. A., Dutkiewicz, S., & Follows, M. J. (2014, 1). Maximal feeding with active prey-switching: A kill-the-winner functional response and its effect on global diversity and biogeography. *Progress in Oceanography*, *120*, 93-109. doi: 10.1016/J.POCEAN.2013.08.001

Walker, N. D., Susanto, H., Steinke, M., & Codling, E. A. (2019). Bottom-up and top-down control in a multitrophic system: the role of nutrient limitation and infochemical-mediated predation in a plankton food-web model. *Communication in Biomathematical Sciences*, *2*, 65-84. doi: 10.5614/cbms.2019.2.2.1

West, G. B., Brown, J. H., & Enquist, B. J. (1997, 4). A general model for the origin of allometric scaling laws in biology. *Science*, *276*, 122-126. Retrieved from https://www.science.org/doi/10.1126/science.276.5309.122 doi: 10.1126/SCIENCE.276.5309.122/ASSET/C437345F-C208-4FBB-993E-E8995AE77F9D/ASSETS/GRAPHIC/122-IMG022.GIF

Westberry, T., Behrenfeld, M. J., Siegel, D. A., & Boss, E. (2008, 6). Carbon-based primary productivity modeling with vertically resolved photoacclimation. *Global Biogeochemical Cycles*, *22*, 2024. Retrieved from https://onlinelibrary.wiley.com/doi/full/10.1029/2007GB003078https://onlinelibrary.wiley.com/doi/abs/10.1029/2007GB003078https://agupubs.onlinelibrary.wiley.com/doi/10.1029/2007GB003078 doi: 10.1029/2007GB003078